Vertical profiles of HDO/H_2O in the troposphere

D. H. Ehhalt and F. Rohrer
Forschungszentrum Jülich, ICG-II: Troposphäre, Jülich, Germany

A. Fried
Atmospheric Technology Division and Atmospheric Chemistry Division, National Center for Atmospheric Research, Boulder, Colorado, USA

Received 3 November 2004; revised 23 February 2005; accepted 31 March 2005; published 1 July 2005.

[1] This paper reanalyzes the measurements of the D content in tropospheric water vapor by Ehhalt (1974) correcting for the isotopic contamination by wall water in the sampling tubes. The resulting corrections decrease the original D content. They are small for the data from the flights through 1967, which extended from the surface to 9 km altitude, but are large for the flights beginning 1971, which ranged from 6 to 13 km altitude and collected smaller amounts of water vapor. No correction therefore was attempted for the latter. The corrected data of the earlier flights are presented in the form of seasonally averaged profiles over Scotts Bluff, Nebraska; Death Valley, California; and the Pacific offshore of San Luis Obispo, California. As to be expected, the vertical profiles from the earlier flights show a decrease in the D content with altitude and a seasonal variation at all altitudes. However, when plotted against the water vapor mixing ratio, the D data from all seasons collapse on a line which closely follows that given by Rayleigh condensation with a fractionation factor $\alpha = 1.1$, constant with altitude. These data can be explained by a simple one-dimensional convection model and the assumption that condensed water is lofted along with the water vapor.

Citation: Ehhalt, D. H., F. Rohrer, and A. Fried (2005), Vertical profiles of HDO/H_2O in the troposphere, *J. Geophys. Res.*, *110*, D13301, doi:10.1029/2004JD005569.

1. Introduction

[2] The isotopic composition of atmospheric water vapor is currently receiving renewed interest, partly because new techniques for its measurement have become available [cf. *Webster and Heymsfield*, 2003] and partly because of its promise of additional insight into the longstanding problems of dehydration in the tropical transition layer, and exchange of air between the stratosphere and the troposphere in general [*Zahn et al.*, 1998; *Keith*, 2000; *Kuang et al.*, 2003; *Dessler and Sherwood*, 2003]. It has, however, been used as a powerful tracer for many other processes in the tropospheric water cycle, among others, to study the growth history of hailstones [*Knight et al.*, 1975], ice particle lofting [*Smith*, 1992], and the formation of precipitation in hurricanes [*Ehhalt and Östlund*, 1970; *Lawrence et al.*, 2002].

[3] All of these applications rest on the fact that the isotopically heavier molecules, in particular deuterated water, HDO, have a substantially lower vapor pressure than the major isotopomer $H_2^{16}O$. This leads to isotopic fractionation between the phases during condensation and evaporation. This fractionation between the vapor phase and the condensed phase is quantified by a fractionation factor α which in thermodynamic equilibrium (and in the case of deuterium, D) is given by

$$R_c/R_v = \alpha = p_{H_2O}/p_{HDO}, \quad (1)$$

where $R = [HDO]/[H_2O]$ is the isotope ratio in the condensed phase c or vapor phase v, and p is the vapor pressure. The fractionation factor α depends on the temperature and is different for ice and liquid (see equations (6) and (7) in section 4.5).

[4] As saturated air is lofted and cooled, the heavy isotopes condense more readily and are removed by precipitation. As a consequence, R_v of the remaining vapor decreases monotonically. In the idealized case of thermodynamic equilibrium and instantaneous removal of the condensate, R_v is described by a simple differential equation:

$$d\ln(R_v) = (\alpha - 1)d\ln(q_v) \quad (2)$$

where q_v is the amount of vapor. Equation (2) is generally called Rayleigh condensation. In the case of a constant α, equation (2) has a simple analytic solution:

$$R_v = R_{v,0}\, f^{(\alpha-1)}, \quad (3)$$

where $R_{v,0}$ is the initial isotope ratio of the water vapor and f is the fraction of vapor remaining. Equations (2) and (3)

0148-0227/05/2004JD005569

capture the salient points of the vertical distribution of the isotope content in water vapor, namely, a monotonic decrease of R_v with the amount of water vapor q_v, and therefore with altitude. In nature this basic process is complicated by a number of physical and meteorological factors, such as supersaturation, the presence of cloud and precipitation droplets, and turbulent mixing within the cloud, which affect the effective α. In turn the measured vertical profiles of the isotope content can provide information about the role of these processes.

[5] Despite the recognition of their utility, there have been only few measurements of the HDO/H_2O or $H_2^{18}O$/$H_2^{16}O$ ratio in tropospheric water vapor, partly because of the cumbersome and time-consuming techniques available in the past.

[6] Here we would like to draw attention to an old set of HDO/H_2O measurements in tropospheric water vapor [*Ehhalt*, 1974]. The set was collected between 1965 and 1973 over various locations in the United States covering an altitude range from 0 to 9 km, later from 6 to 13 km, and is unique in the sense that it provides full annual climatologies. It has already been used by various authors [e.g., *Rozanski and Sonntag*, 1982; *Gedzelman*, 1988; *Smith*, 1992; *Zahn et al.*, 1998], despite the fact that the data were somewhat hidden in a National Center for Atmospheric Research (NCAR) technical note which reported raw data only. The data are based on water vapor samples which were trapped cryogenically by passing ambient air through dry ice or liquid nitrogen cooled U-tubes. This method of collection invariably faces the problem of contamination of the isotopic signature in the collected water vapor by water adhering to the inner surfaces of the sampling system prior to collection. This effect was not accounted for in the published raw data.

[7] As we will show in the present paper, this contamination becomes significant for ambient air samples with a water vapor content of less than 0.1 g H_2O/kg air, or for altitudes higher than 7 km. Thus, to extend the usable altitude range of the data set upward, we also develop a procedure to correct for the contamination by wall water. The changes introduced by the correction are illustrated by comparison of the seasonally averaged profiles from the original data with those from the corrected ones. We also discuss the major features of the averaged seasonal vertical profiles of the corrected D content and compare them with those derived from one-dimensional (1-D) model simulations.

2. Flights and Sample Collection

[8] Monthly sampling flights began in November 1965 over Scottsbluff, Nebraska, at 41°50′N, 101°40′W, and 1.2 km above sea level using the NCAR Queen Air 80. From February to June 1966, about three profiles were obtained each month. The samples were collected at eight altitudes: 1.52, 1.83, 2.29, 3.05, 4.47, 6.1, 7.62, and 9.15 km above sea level, with sampling times ranging from 15 min at the lowest altitudes to 1 hour at the four highest altitudes. Each profile required two aircraft flights. Sampling was done in clear air; no flights were made in completely overcast situations, although on a few occasions, when flying between clouds, condensed water was collected. The Scottsbluff flights were terminated in January 1967.

[9] In July 1966 a series of monthly flights was begun over the Pacific, about 34°N, 125°W, 200 km west of San Luis Obispo, California, and over Death Valley, 36°N, 117°W, about 300 km inland. Initially eight altitudes were sampled, but later only seven were sampled because of the limited fuel capacity of the aircraft (for details, see *Ehhalt* [1974]). This program ended in August 1967.

[10] From March 1971 to September 1973, NCAR's Sabreliner was used to extend the earlier flights over Scottsbluff to higher altitudes with sampling altitudes and sampling times of 6.4 km (10 min), 7.6 km (15 min), 8.8 km (20 min), 10 km (20 min), 11.3 km (20 min), 11.9 km (30 min), and 13.1 km (30 min). Since flight time available on the Sabreliner was limited, the flight dates were irregular. In particular, no flights during June and July could be obtained, limiting annual coverage. A few flights were made at other locations, some of which extended to the surface: Two oceanic flights, one each over the east and west coasts, were made for comparison. Three profiles were obtained over east Texas when the Sabreliner was available to support NCAR's stratospheric balloon flights over Palestine, Texas.

[11] During the earlier flights, until 1967, water vapor for the isotope analysis was collected by passing the ambient air through U-tubes that were cooled in a mixture of dry ice and solvent. The U-tubes were made of stainless steel tubing 5 cm in diameter and 1 m in length. Before and after collection each U-tube was closed by vacuum valves. A stainless steel frit of 60 μm pore size and 40 cm^2 area was mounted at the exit of each U-tube to retain ice crystals that might form in the air stream during rapid cooling of moist air. The efficiency of water vapor collection and the integrity of the isotopic content of the collected water were checked in the laboratory by measuring the amount and D content of water vapor frozen out in the U-tubes at various flows and pressures and comparing these measurements with those obtained in a Horibe trap operated in parallel at a fixed flow of 1 L/min. The agreement was excellent up to a flow of 40 L/min.

[12] The air intake was mounted on the top forward section of the Queen Air fuselage to avoid contamination by engine exhaust and extended out 20 cm from the hull into the free airstream. It was connected to the U-tubes with a polyethylene tubing 2 cm in diameter. Suction was provided by a set of venturis at the side of the aircraft to maintain a flow of 35 L/min through a U-tube at all altitudes. At the two highest altitudes, air was passed through two U-tubes in parallel to double the sampling rate. The flow rate was measured by a "vol-o-flow" flow gauge and recorded during the flight. Air pressure and temperature of the flow were measured with a Wallace and Tiernan gauge (600 torr full scale) and a thermoelement, respectively. A valve connecting the intake line with the exhaust line allowed airflow bypassing the U-tubes to flush the inlet line between the samples.

[13] For the recovery of the ambient water vapor collected, the U-tubes were returned to the laboratory where they were individually connected to a vacuum line and evacuated while cold. They were then brought to room temperature with the help of a heat gun, and the water vapor was

distilled over into liquid nitrogen cooled ampoules in which the samples could be weighed and stored. At room temperature a small but significant amount of water remains on the walls of the U-tubes (see section 3). Typical (median) amounts of water recovered ranged from 3 g at ground level to 0.1 g at 9.15 km altitude. The ambient water vapor mixing ratios were calculated from the flow rate, pressure, sampling time, and the collected amount of water with a relative error of less than ±5%.

[14] The Sabreliner flights 1971–1973 reached much higher altitudes and therefore encountered smaller water vapor mixing ratios; thus liquid N_2 was used as coolant to ensure quantitative collection. In addition, because the available flight time was much shorter, a sampling system allowing much higher flow rates had to be employed to collect adequate amounts of water vapor. It consisted of eight stainless steel collection vessels mounted on one flange and submerged in a slightly pressurized liquid N_2 dewar. Each vessel was 80 cm long and 7.5 cm in diameter and consisted of three concentric tubes. The flow was forced downward along the gap between the outer tube and middle tube whose lowest 10 cm consisted of a stainless steel frit of 200 cm^2 surface; the flow then entered the gap between the middle and inner tubes where the air flowed upward. Both inner and outer tube walls were in contact with the liquid N_2. These vessels allowed flows up to 120 L STP/min without loss of water vapor, as checked by a series of laboratory experiments at different flow rates and pressures. The vessels were connected by vacuum valves to inlet and outlet manifolds which in turn were connected by stainless steel flexible tubes of 2.5 cm diameter to the intake and outlet on the fuselage. In flight the ram pressure was used to maintain the flow. Monitoring of the flow and recovery of the water vapor samples was similar to that described for the U-tubes used earlier except that the tubes were heated to about 80°C for sample transfer.

[15] For the measurement of the HDO/H_2O ratio, aliquots of the recovered water were converted to H_2 by reduction over hot depleted uranium. The H_2 was then injected into an Atlas MS86 mass spectrometer for isotopic analysis following the usual analytic procedures at that time [cf. *Friedman*, 1953]. The D content is expressed as a δ value, which is defined as relative deviation of the HDO/H_2O ratio R, of the sample SA, from that of Standard Mean Ocean Water, SMOW, in per mil [*Craig*, 1961]:

$$\delta_{SMOW} = [(R_{SA} - R_{SMOW})/R_{SMOW}] \times 1000. \quad (4)$$

[16] The standard deviation of the D content introduced by the mass spectrometric measurement was ±1‰. As we shall see below, most of the error in the measured D content of tropospheric water vapor comes from other sources and can be much larger.

3. Correction for Wall Water

[17] The water eventually recovered from the sampling tubes is isotopically contaminated by water adsorbed on the inner walls of the sampling and recovery system. Since the inlet line was flushed with ambient air prior to sample collection, its contribution to the isotopic contamination of the recovered water is small. Most of the contamination is expected from the sampling tubes themselves with a smaller contribution from the recovery system owing to its smaller inner surface area. The recovery procedure, evacuation and transfer times, followed the same protocol for all flights and all tubes. Thus the amount of wall water on the inner surfaces of each individual tube should have remained unchanged after each sampling and recovery sequence. The same holds for the amount of wall water in the recovery line. Because the tubes were identical, the amounts of wall water should also have been the same in all tubes. By the same token, the amounts of water recovered should have equaled the amounts of water vapor collected. The isotopic content of the recovered water, however, is changed with respect to the collected water vapor. Because the contact times were long enough for isotopic exchange, the D content measured in the recovered water, δ_m, rather represents the amount weighted mixture of the D content in tropospheric water vapor, δ_v, and that of the various contributions from the inner surfaces it was exposed to δ_w:

$$\delta_m = \delta_v \times q_v/(q_v + q_w) + \delta_w \times q_w/(q_v + q_w), \quad (5)$$

where the indices v and w refer to tropospheric water vapor and wall water, respectively. Here q is the respective amount of water, and we underline that q_v is given by the recovered amount of water.

[18] Unfortunately, the procedures employed in the aircraft sampling were not tested for the recovery of very small amounts of water. Neither the amount of wall water nor its D content was determined in separate experiments, as had been done, for example, in the later balloon flights [*Ehhalt et al.*, 2002]. Nor were the tubes preconditioned with water of known D content to ensure reproducibility in the D content of the wall water. Thus amount and D content of the contaminant wall water have to be estimated.

[19] Fortunately, the sampling procedure also followed a protocol inasmuch as the sampling tubes were kept evacuated and sealed when in storage, and sampling aboard the aircraft followed the same altitude sequence such that a given altitude was generally sampled by the same tube. This together with the information given in section 2 allows one to estimate (1) the average amount of wall water and (2) its D content. In the following we provide estimates for each of these and show how they translate into a correction.

[20] The amount of wall water can be estimated from the inner surface area exposed to the samples. With a length of 1 m and an inner diameter of 5 cm the walls of the U-tubes contribute a surface of 1610 cm^2. A much larger contribution comes from the frit. Assuming that it is sintered from stainless steel spheres of 100 μm diameter to produce pores of 60 μm, and that the frit has a thickness of 1 mm, its total surface area is 2400 cm^2. A monomolecular layer of H_2O contains about 5×10^{14} molecules/cm^2, and at room temperature about 60 layers of water molecules are adsorbed on a clean stainless steel surface [*Dushman*, 1962]. Thus a total of about 1.2×10^{20} H_2O molecules or 3.6 mg of H_2O should theoretically be adsorbed on the inner walls of a U-tube. *Zahn* [1995] has shown that for his water vapor traps, which, similar to ours, were also made of stainless steel, the actual amount of water adsorbed was about a factor of 5 larger than its theoretical estimate, which was calculated analogous the present one. Thus we assume

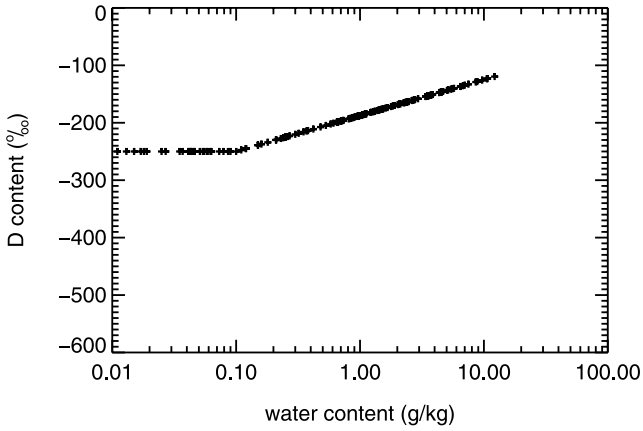

Figure 1. The average D content of wall water, δ_w, plotted as function of the water vapor mixing ratio q_v.

a value of 20 mg for the H_2O adsorbed on the inner walls of the U-tubes (including the recovery line) as our reference case and assign it an error of ±10 mg. The amount of air passed through the U-tubes during sampling was about 1 kg for the altitudes above 3 km. Thus 20 mg of wall water correspond to a contribution of 0.02 g/kg air in water vapor mixing ratio.

[21] Concerning the D content of wall water, we will assume that the wall water represents a 1-to-1 mix of wall water retained from the previous flight and water vapor from the laboratory leaking into the U-tubes during storage. The wall water resulting from laboratory air has a D content of about −100‰ [*Ehhalt et al.*, 2002]. The D content of the water remaining from the previous flight depends on sampling altitude or more precisely on the water vapor mixing ratio in the air sampled (see Figure 4 below). It was derived by fitting a straight line to the dependence of the measured D content, δ_m, on the logarithm of the measured water mixing ratio for all data collected through 1967, and assuming a constant value of −400‰ at humidities $q_v <$ 0.1 g/kg air (compare Figure 4c). The resulting profile of the D content in wall water is shown in Figure 1. We will assign

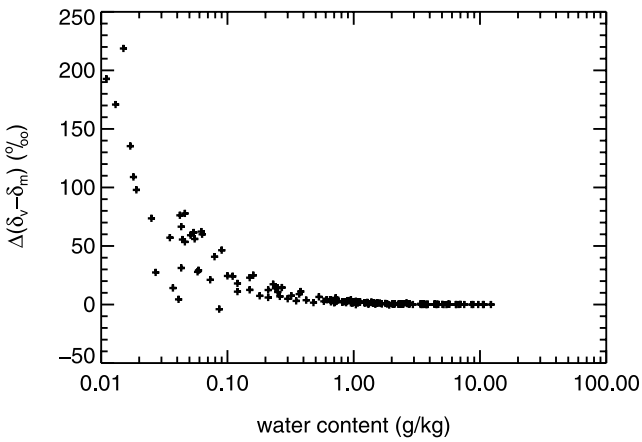

Figure 2. The correction for wall water contamination, defined as $\delta_v - \delta_m$, plotted as function of the water vapor mixing ratio, q_v, for the data over Scotts Bluff, 1965–1967.

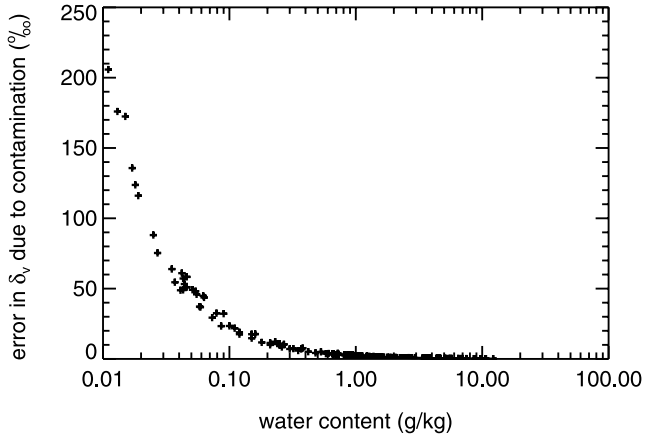

Figure 3. The uncertainty (2σ) of the corrected D content, δ_v, in an individual sample due to wall water contamination plotted as function of the water vapor mixing ratio, q_v, for the data over Scotts Bluff (see text).

an error of ±100‰ to the D content of wall water for all altitudes sampled.

[22] With this information, all needed parameters are known, and we can solve equation (5) for δ_v, the actual D content of the sampled tropospheric water vapor. This constitutes the required correction for wall water contamination. It is applied for each sample individually based on the respective δ_m, δ_w, and q_v. To illustrate the magnitude of this correction, the difference between δ_v and the measured (and originally published) D content δ_m is shown as a function of q_v for the samples from the flights over Scotts Bluff, 1965–1967 (Figure 2).

[23] We note that the corrections remain negligible for water vapor mixing ratios, q_v, between 10 and 0.5 g/kg air. Below that q_v they begin to increase gradually to an average of −30‰ at 0.1 g/kg air, but then rise rapidly to a value of −200‰ at q_v 0.01 g/kg air. We also note that the large majority of the samples requires corrections of less than 50‰; for Scotts Bluff only five out of a total of 156 need a correction of more than 100‰.

[24] With the lack of experimental evidence it is difficult to quantify the error in these corrections and thus that of δ_v due to wall water contamination. To illustrate its possible magnitude, we propagate the errors assigned to q_w and δ_w via equation (5) into δ_v. This leads to the dependence of that error on q_v depicted in Figure 3. Clearly the error is large, of the same order as the correction itself.

[25] However, from a consistency check based on the derived vertical profile of δ_v for Scotts Bluff, we will argue in section 4.3 that the error given in Figure 3 represents the 2σ bounds. Since the measurement errors in δ_m and q_m are comparatively small, the errors from the wall water contamination in Figure 3 also define the total error in δ_v.

[26] In principle, the data from the later Sabreliner flights should also be corrigible. There are, however, several obstacles. In this case the inner surfaces of the sampling tubes were much larger and more uncertain, since the thickness of the frits is no longer on record. This increases the wall water by a substantial but uncertain amount. (On the other hand, the tubes were heated to 80°C during

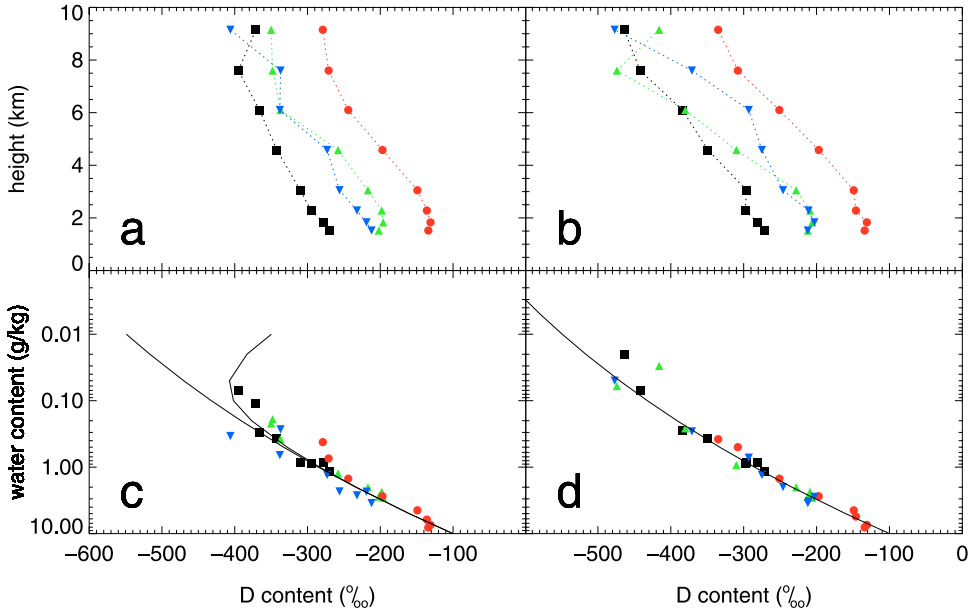

Figure 4. Seasonally averaged vertical profiles of the D content in tropospheric water vapor and the corresponding dependence of the D content on the observed water vapor mixing ratio for Scotts Bluff, 1965–1967. Figures 4a and 4c represent the original data; Figure 4b and 4d represent the corrected data. Legend is winter, squares; spring, upward pointing triangles; fall, downward pointing triangles; summer, circles. The solid lines in Figures 4c and 4d represent the Rayleigh condensation curve with $\alpha = 1.1$. A second full curve in Figure 4c represents a Rayleigh curve contaminated with 0.02 g/kg air of wall water with the varying D content from Figure 1.

recovery, which reduces the wall water retained and partly compensates for the larger surface area.) Moreover, these flights sampled higher altitudes with lower moisture contents, and thus collected less water. As a consequence, the corrections for the Sabreliner flights (and their errors) can become exceedingly large; in fact, in several cases they lead to unphysical values of $\delta_v < -1000‰$. Thus we conclude that the present method does not lend itself to the correction

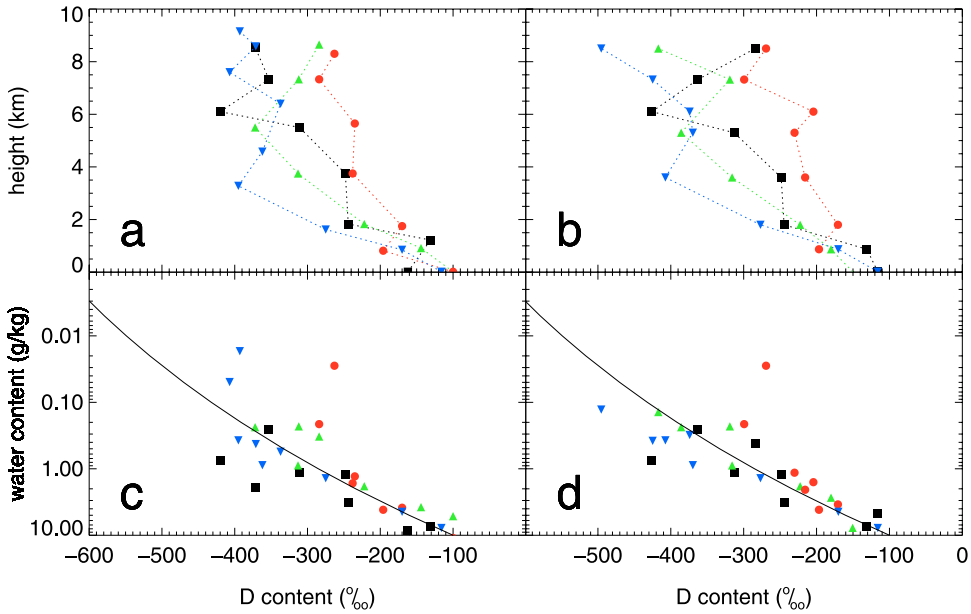

Figure 5. Seasonally averaged vertical profiles of the D content in tropospheric water vapor and the corresponding dependence of the D content on the observed water vapor mixing ratio for the Pacific, 1966–1967. Figures 5a and 5c represent the original data; Figures 5b and 5d represent the corrected data. Legend is winter, squares; spring, upward pointing triangles, fall, downward pointing triangles; summer, circles. The solid lines in Figures 5c and 5d represent the Rayleigh condensation curve with $\alpha = 1.1$.

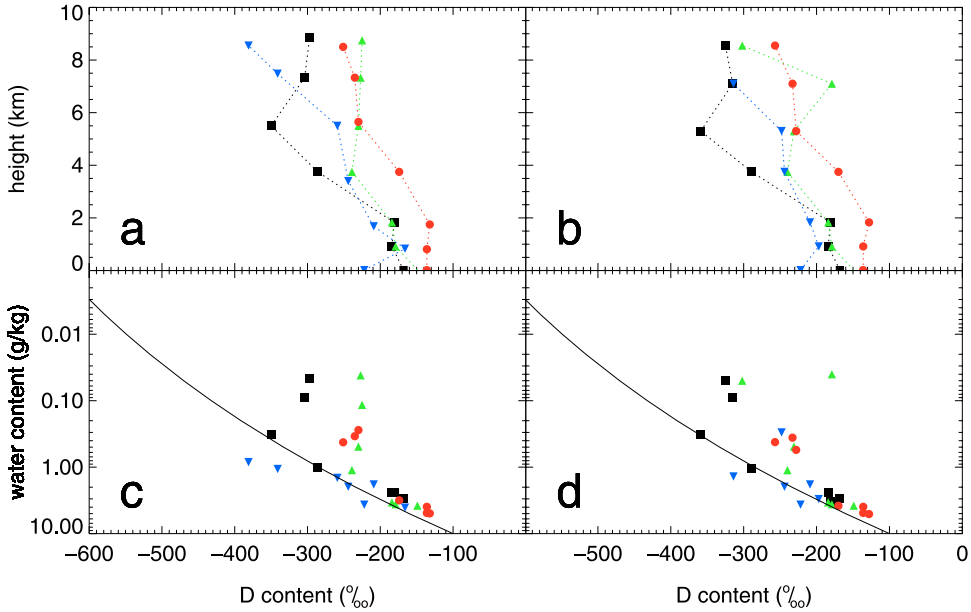

Figure 6. Seasonally averaged vertical profiles of the D content in tropospheric water vapor and the corresponding dependence of the D content on the observed water vapor mixing ratio for Death Valley, 1966–1967. Figures 6a and 6c represent the original data; Figures 6b and 6d represent the corrected data. Legend is winter, squares; spring, upward pointing triangles; fall, downward pointing triangles; summer, circles. The solid lines in Figures 6c and 6d represent the Rayleigh condensation curve with $\alpha = 1.1$.

of the data collected between 1971 and 1973, and we did not attempt to do so.

4. Results and Discussion

[27] In the following we take a first look at the average, climatological features of the measured and corrected D content in tropospheric water vapor above the three locations: Scotts Bluff, Nebraska, Death Valley, California, and the Pacific, 200 km west of San Luis Obispo. The original and corrected data are now available at http://www.atd.ucar.edu/apol/ehhalt/Vertical_Profiles_of_HDO.html.

4.1. Seasonally Averaged Profiles

[28] The data from a given location and altitude are seasonally averaged; a season consists of three months, winter representing the months December, January, and February. Because the altitudes had to be changed during the course of the flight series (see *Ehhalt* [1974] for details), the data are binned into altitude intervals before averaging and assigned to the average altitude of the respective interval.

[29] For Scotts Bluff from 1965 to 1967, four to seven flights are available per season. Sampling over Death Valley and the Pacific is less frequent, with two to four flights per season.

[30] Besides correcting the data for wall water contamination by the procedure outlined in the previous section, we also omitted all data with relative humidities $h > 100\%$, to eliminate samples possibly containing cloud or precipitation particles. This removes 22 data points from the original total of 323, or about 7% of the flights through 1967. As a consequence a few altitude bins are empty or contain one measurement only. The resulting average height profiles of the corrected D content, δ_v, are summarized in Figure 4 for Scotts Bluff and in Figures 5 and 6 for the Pacific and Death Valley. Since the D content depends primarily on the fraction of water vapor left after condensation, the dependence of δ_v on the measured water vapor mixing ratio, q_v, is also shown in Figures 4, 5, and 6. A common reference curve allows comparison between the δ_v/q_v dependences at the different locations. It is based on Rayleigh condensation with a constant fractionation factor, $\alpha = 1.1$, and $\delta_{v,0} = -100‰$ and a water vapor mixing ratio $q_{v,0} = 10$ g/kg as the lower boundary values.

[31] To illustrate the impact of the correction for wall water, the average profiles from the full set of the original data are also shown for all locations. The standard deviations in the seasonally averaged D and water vapor content are considerable, up to ±100‰ in δ_v, and up to about a factor of 2 in water vapor (see Figure 9 below). Most of it is due to the natural variability in the D content and water vapor mixing ratio. For clarity the error bars are omitted in Figures 4, 5, and 6.

4.2. Seasonally Averaged Profiles Over Scotts Bluff

[32] The vertical profiles of the D content over Scotts Bluff clearly exhibit the expected general decrease with altitude (Figure 4). They also show the expected seasonal variation with higher D contents during summer. Smaller-scale structure superimposed on the monotonic vertical decrease of the D content is mostly due to the variance in the observed water vapor mixing ratio. Plotting the D content against the water vapor mixing ratio removes virtually all of that structure. Interestingly, in the case of Scotts Bluff, that plot removes also all of the seasonal variation and leads to a narrow clustering of the seasonal averages along a single line virtually coinciding with our reference curve. This means that the average local vertical

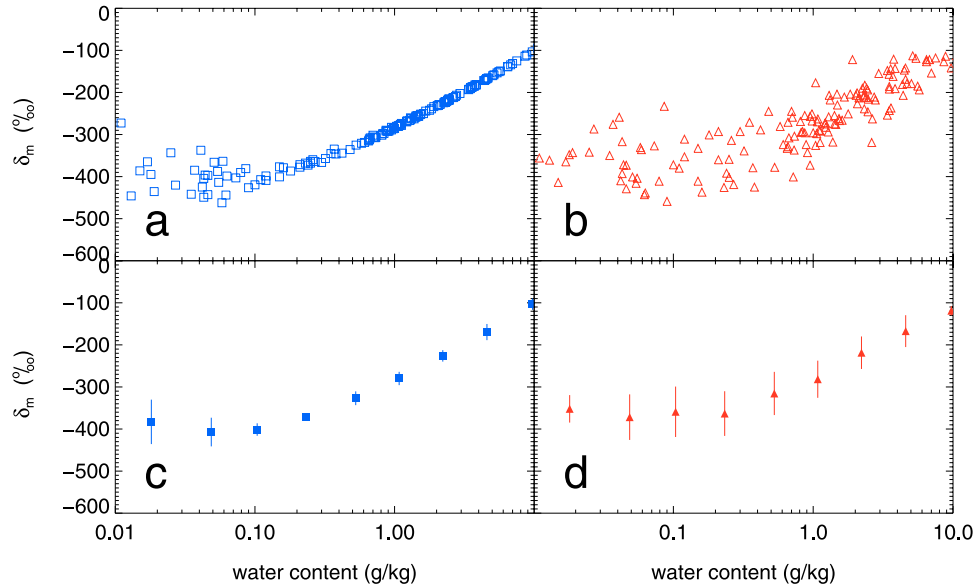

Figure 7. Comparison of simulated and measured δ_m for all Scotts Bluff data from 1965–1967 with h < 100%. (a) Scatterplot of the simulated δ_m versus the measured water vapor mixing ratio, q_v. (b) Scatterplot of the measured δ_m versus q_v. (c) Averaged simulated δ_m and its standard deviation versus averaged q_v. (d) Averaged measured δ_m and its standard deviation versus averaged q_v.

distribution of δ_v depends only on q_v. In particular, it has the same functional dependence on q_v in all seasons; moreover, the seasonal lower boundary values, $\delta_{v,0}$, have the same dependence as well. Since winter and summer precipitation is caused by different processes, which operate at different temperatures and thus with different $\alpha(T)$, this finding is rather unexpected. Equally unexpected is the observation that this dependence seems to follow a Rayleigh condensation curve with a constant α for all seasons and all altitudes observed.

4.3. Consistency Check

[33] The tight and unequivocal δ_v/q_v relation for the seasonally averaged Scotts Bluff data also allows a consistency check on our correction procedure. With a known δ_v/q_v relation we can simulate the impact of wall water on the measured δ_m using equation (5). To also obtain the variance on δ_m introduced by the uncertainties in the amount and D content of wall water in the individual samples, we allow q_w to vary around the mean of 0.02 g/kg air with an Gaussian distribution with a σ of 0.01 g/kg air, and δ_w to vary around the mean defined by the curve in Figure 1 with a σ of 100‰. For simplicity we assume δ_v/q_v to follow the reference Rayleigh curve in Figure 4d. We note, however, that this reference curve although closely describing the data does not represent a fit. The results of the simulation are summarized in Figure 7. Figure 7a shows the scatterplot δ_v versus q_v for the 156 simulated Scottsbluff data points with h < 100%. The scatter due to the uncertainties in the wall water contamination become noticeable for humidities q_v < 0.3 g/kg air. Above that value the influence of wall water is to small to change δ_v, and the simulated δ_m follow exactly the reference curve. This is in contrast to the corresponding measured δ_m in Figure 7b, which exhibit large scatter for all humidities indicating, not unexpectedly, that there are natural factors besides q_v that influence the D content in the individual samples of tropospheric water vapor. For better comparison, Figure 7 also includes the δ_m versus q_v profiles averaged over the individual data and their standard deviations (Figure 7c for the simulated, Figure 7d for the measured δ_m). They were obtained by binning both data sets with respect to q_v into the intervals: q_v < 0.03; 0.03 < q_v < 0.07; 0.07 < q_v < 0.3; 0.3 < $q_{v<}$ 0.7; etc., and averaging δ_m and q_v in each bin.

[34] The measured and simulated average δ_m versus q_v profiles have the same form and agree well within the respective standard deviations. The standard deviations, however, exhibit quite different dependences on q_v. Apart from the larger variance of the measured δ_m at q_v > 0.3 g/kg air, the standard deviation in the measured δ_m decreases for

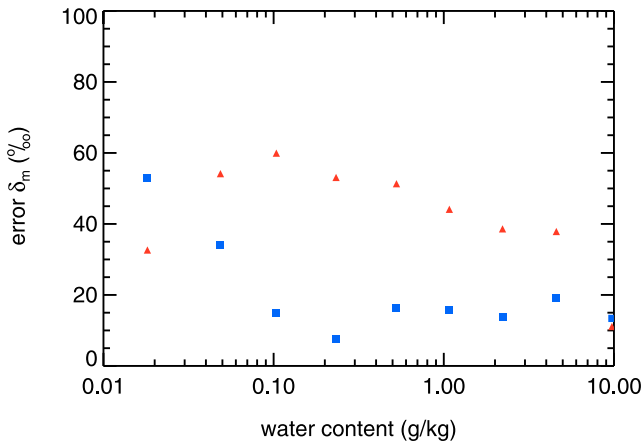

Figure 8. Dependence of the standard deviations in the simulated (squares) and measured (triangles) δ_m on the measured water vapor mixing ratio, q_v.

the lowest three q_v, whereas that of the simulated δ_m increases. This is more clearly shown in Figure 8, which presents the standard deviations as a function of q_v. The decrease in the variance of the measured δ_m is difficult to explain; part of it may be fortuitous or even reflect a real atmospheric feature, and another part must be due to the fact that the sampling times in the highest altitudes were longer and that therefore these samples represent averages over larger air volumes. The increase in the standard deviation of the simulated δ_m is as expected and due to the increase in correction with decreasing q_v (see also Figure 3). In any case this different behavior leads to the apparent paradox that for the lowest q_v the standard deviation in the simulated δ_m is larger than that of the measured δ_m and nearly equal for the next lowest q_v. Since the variance in the measured δ_m includes that induced by wall water contamination, it should always be larger than the variance in the simulated δ_m. Thus we are led to the conclusion that the standard deviations for q_w and δ_w tentatively introduced in section 3 are too large. Comparison of the standard deviations of 53‰ in the simulated and of 33‰ in the measured δ_m at the lowest q_v suggests an overestimate of the error induced by wall water by at least a factor of 1.6. Since the standard deviation in the measured δ_m must include some natural variability, a factor of 2 is more likely. The error analysis in section 3 leading to Figure 3 also shows that for the lowest q_v the uncertainty in δ_w contributes about a factor of 1.8 as much to the total error due to wall water contamination than that of q_w. Thus it is essentially the error in δ_w that had been overestimated in section 3. Owing to lack of information, a more quantitative attribution of error is not feasible.

4.4. Seasonally Averaged Profiles Over the Pacific and Death Valley

[35] Figure 5 summarizes the isotopic data over the Pacific. The vertical profiles of δ_v (Figure 5b) show considerably more scatter than the Scotts Bluff data. As a consequence, although still present, vertical decrease and seasonal variation are not as clearly expressed as over Scotts Bluff. There are two reasons for the large scatter: (1) There are about a factor of 2 fewer data available over the Pacific; consequently the standard deviations of the seasonal averages are larger. (2) The sampling area is only 200 km from the shoreline. The profiles are therefore influenced by continental as well as maritime air masses, which are expected to carry different isotopic signatures and thus add variability at a given altitude.

[36] In addition, the sea surface temperature remains comparatively constant throughout the year. Thus water vapor in isotopic exchange with it will show little isotopic variation with season and the D content in the lowest two altitudes does not vary significantly with season.

[37] Nevertheless, when plotted against q_v, the seasonally averaged δ_v tend to follow the reference line, consistent with the Scotts Bluff data, although with a much larger scatter. The scatter is in fact large enough that we cannot exclude the possibility of a small seasonal variation in this δ_v versus q_v plot.

[38] The seasonally averaged vertical profiles over Death Valley (Figure 6) also show more scatter than those over Scotts Bluff, mostly due to the smaller database. Even though, the general decrease of δ_v with altitude and its seasonal variation are clearly visible. The vertical gradients at the highest altitudes, however, are smaller than those observed over Scotts Bluff and the Pacific. For example, the summer profile over Death Valley above 5 km decreases much more slowly than that over Scotts Bluff, whereas it is virtually identical for the altitude range between 1 and 5 km above sea level. The fall and spring profiles too show a slower decrease above 5 km altitude but are similar below. This observation translates into the δ_v versus q_v plot (Figure 6d). Only the lowest part, i.e., samples with $q_v >$ 1 g/kg air, follow the reference line. Most samples from all seasons with $q_v <$ 1g/kg air follow a much weaker gradient. It looks almost as if the δ_v/q_v dependence consisted of two separate parts. Comparison with Figure 6b indicates that the transition point, $q_v \sim$ 1g/kg air, corresponds to about 4 to 5 km altitude. This may provide a hint for the reason of the two branches. Given the dryness (see also q_v in Figure 6d) and the lack of precipitation over Death Valley, the vertical decrease in δ_v is not generated locally but rather is dominated by advection. Thus it could well be that the upper branch of the δ_v/q_v dependence is shaped by the passage of the Pacific storms over the Sierra Nevada mountain range. In any case the profiles over Death Valley provide an example of a clear deviation from the reference curve.

[39] Figures 4, 5, and 6 also demonstrate the result of the correction for wall water contamination. It is essentially limited to the data with the lowest water vapor mixing ratios, i.e., to the highest altitudes, and lowers δ_v with respect to δ_m. Changes in the seasonally averaged profiles at altitudes below 7 km are mostly caused by the omission of data with h > 100%. On the whole, the correction increases the vertical gradient in the D content, but it does little to remove the scatter in the height profiles.

[40] This is different for the dependence of δ_v on q_v, where the correction not only steepens the slope but also removes some of the scatter.

4.5. Simulation by One-Dimensional Models

[41] To gain some insight into the factors controlling the observed δ_v/q_v dependence, in particular to explain its closeness to the reference Rayleigh curve in the case of Scotts Bluff, we will attempt to simulate the D content and the water vapor mixing ratio by simple one-dimensional models.

[42] Since boundary and initial conditions change with location and season, we consider one location, Scotts Bluff, and one season, summer, in our model runs. The lower boundary conditions are adjusted to the observed average values: D content $\delta_{v,0} = -134$‰, water vapor mixing ratio $q_{v,0} = 8$ g/kg, temperature $T_0 = 23$°C. We assume a constant lapse rate of 6.5°C/km for the vertical temperature profile and a pressure of 877 hPa at the lowest altitude of 1.2 km above sea level (asl), decreasing with a scale height of 7 km. The tropopause is at 12 km with a constant temperature of 220 K above. The upper boundary is at 14 km with a D content of $\delta_{v,u} = -650$‰ and a water vapor mixing ratio, $q_{v,u} = 5$ ppmv, corresponding to literature values [*Kuang et al.*, 2003; *Kley et al.*, 2000]. The upper boundary conditions are of little impact on the profiles.

[43] Two types of models were run: The first type, called C for convection, facilitates vertical transport by lofting air from the surface layer directly into a randomly selected

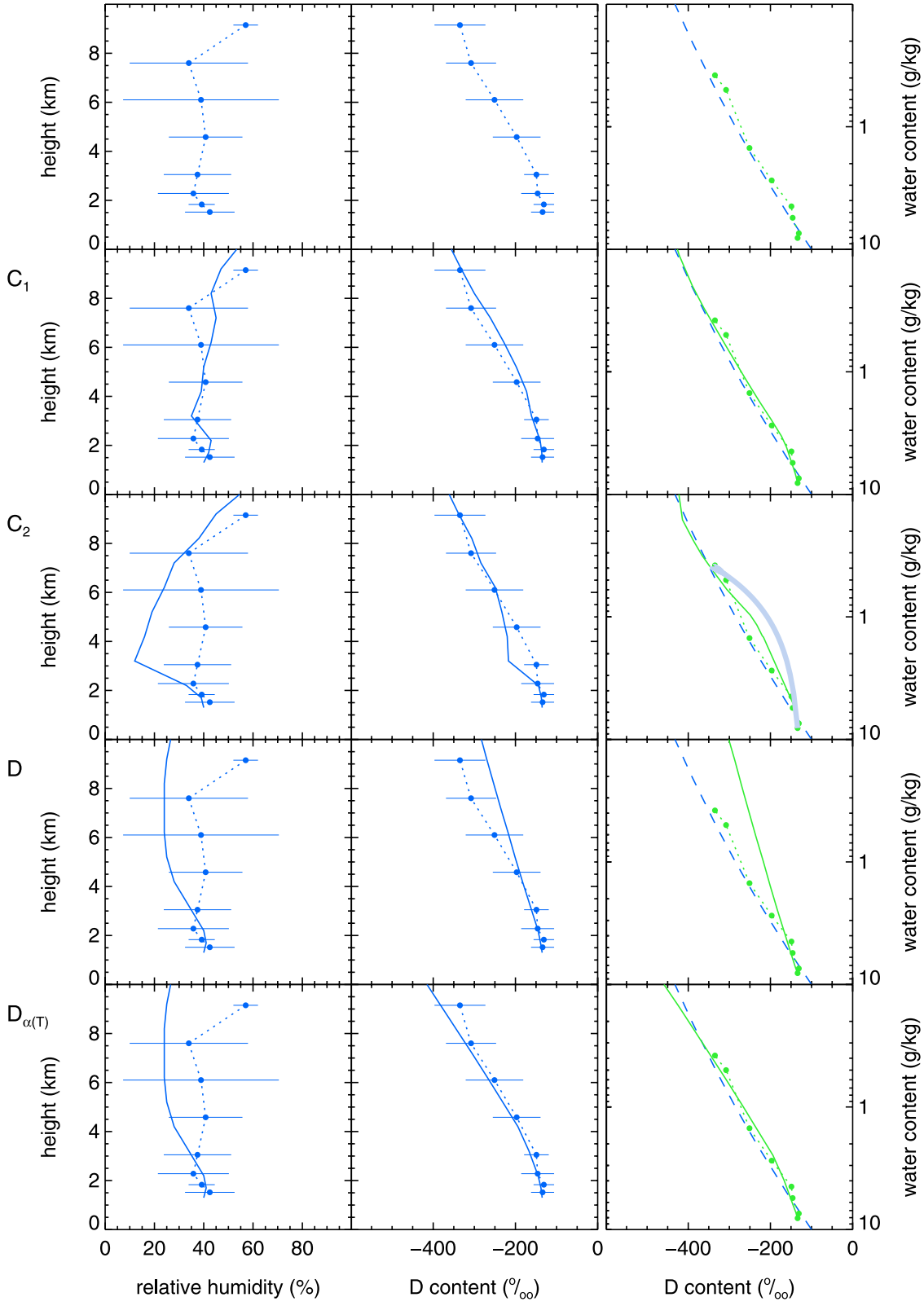
C1
C2
D
Dα(T)
height (km)
water content (g/kg)
relative humidity (%)
D content (‰)
D content (‰)
0 20 40 60 80
−400 −200 0
−400 −200 0
0 2 4 6 8
1 10

Figure 9

altitude between 1 and 12 km [see *Ehhalt et al.*, 1992]. The lofted air induces a corresponding downward displacement of air in the layers below continuing to the surface, to conserve air mass. This generates a certain degree of vertical mixing. The water vapor mixing ratio injected at altitude is reduced to the vapor pressure over water or ice, respectively, corresponding to the prescribed temperature profile. Its D content is calculated by Rayleigh condensation, where the fraction of the remaining water vapor, f, is given by the ratio of the vapor pressure at altitude, p_{H_2O}, to that in the surface layer, $p_{H_2O,0}$ corresponding to $q_{v,o}$. At the lowest altitudes, where p_{H_2O} exceeds $p_{H_2O,0}$, f = 1. Two injection profiles were used: C1, injecting air at all altitudes with the same rate, corresponding to a turnover time at each altitude of 23 days, i.e., the air at the target altitude is replaced by air from the surface layer every 23 days; and C2, which injects air essentially into the uppermost 2 km of the troposphere with a turnover time of 2.3 days. The air in the two layers below is turned over in 11.5 days and in the farther layers down to 4 km in 23 days only. A constant fractionation factor, $\alpha = 1.1$, was used. To mix the boundary layer, a constant eddy diffusion coefficient of 10 m^2/s was introduced between the surface layer and 1 km altitude. The two uppermost layers, 12 to 14 km, representing the lower stratosphere, were mixed with an eddy diffusion coefficient of 1 m^2/s.

[44] The second type model, D, provides vertical transport by eddy diffusion only with an eddy diffusion coefficient profile of 10 m^2/s up to 1 km, 4 m^2/s between 1 and 12 km, and 1 m^2/s between 12 and 14 km. Water vapor is removed in the troposphere with a uniform lifetime of 13 days to generate a water vapor profile exponentially decreasing with the same characteristic height as the observed one. HDO is removed by a lifetime that is smaller by the factor α. Two profiles of α were run in this case: constant $\alpha = 1.1$, as before, and a temperature dependent $\alpha(T)$ corresponding to equations (6) and (7) for the vapor/water and vapor/ice equilibrium after *Majoube* [1971] and *Merlivat and Nief* [1967], respectively:

$$\alpha_L(T) = \exp\left(24844/T^2 - 76.248/T + 0.052612\right) \quad (6)$$

$$\alpha_I(T) = \exp\left(16288/T^2 - 0.0934\right). \quad (7)$$

Transition between the two $\alpha(T)$ was assumed at T = 270 K.

[45] The results from the runs C1, C2, D, and $D_{\alpha(T)}$ are summarized in Figure 9 and compared with the observed vertical profiles of relative humidity (which brings out the differences more clearly than a profile of the water vapor mixing ratio) and of the D content, as well as with the observed dependence of the D content on the water vapor mixing ratio.

[46] Practically all of the model runs fit the observed vertical profile of δ_v over Scotts Bluff within the error bars, which are rather large. Thus it may appear that the data are not precise enough to differentiate between the model runs. The crucial test, however, is the δ_v/q_v dependence. It places a much stronger constraint on the models. The reason is that at any given altitude the variance in the observed δ_v is correlated with the variance in q_v (i.e., higher D contents are associated with higher water vapor mixing ratios) and that this correlation has virtually the same functional form as the overall δ_v/q_v dependence. As a consequence the scatter of the data points around the average curve of the δ_v/q_v dependence is much smaller than indicated by the error bars shown for δ_v alone. This dependence therefore does provide a stringent model test.

[47] Out of the four, only run C_1 and $D_{\alpha(T)}$ fit the observed δ_v/q_v dependence well. This serves to demonstrate that quite different choices in the mode of transport and the profile of α can lead to a satisfactory fit. In turn this means that a successful fit of the δ_v/q_v dependence does not by itself unequivocally determine the proper mode of transport or choice of α. Additional information is needed. In the present case the vertical profile of the relative humidity, h, gives a first clue. The h profile is reasonably well simulated by C_1 but not by $D_{\alpha(T)}$. Another argument against $D_{\alpha(T)}$ is that it would not fit well the δ_v/q_v dependence during winter: Because temperatures are much lower and thus $\alpha(T)$ significantly higher, $D_{\alpha(T)}$ produces a steeper slope than observed over Scotts Bluff (see Figure 4d). The main point, however, is that the fractionation within a cloud acts with an effective α^* that is significantly smaller than $\alpha(T)$, as will be discussed in section 4.6. Thus the combination of $\alpha(T)$ and transport by pure eddy diffusion is not likely to be realistic.

[48] Incidentally, a run with the injection profile of C1 but $\alpha(T)$ would generate a δ_v/q_v relation essentially coincident with that for C1 down to water vapor mixing ratios of 1 g/kg, but increasingly deviating at lower humidities, reaching $\delta_v = -508‰$ instead of $\delta_v = -432‰$ at a water vapor mixing ratio of 0.1 g/kg. It thus does not provide as good a fit to the observations as C1.

[49] This leaves C_1 as a possible solution. It explains all three of the observed profiles reasonably well.

Figure 9. Comparison of the model generated profiles of humidity and D content with the observations for summer over Scotts Bluff, 1965–1967. The left column of panels represents the vertical profiles of the relative humidity, the middle column represents the vertical profiles of the corrected D content, δ_v, the right column represents the dependence of δ_v on the water vapor mixing ratio. The solid lines indicate the model results, the dots indicate the observed data points, and the bars represent the standard deviation in the observations. The dashed lines in the right column represent the Rayleigh condensation curve with $\alpha = 1.1$. The top row shows the data only connected by dotted lines. The next two rows show also the convective model runs C_1 and C_2, with $\alpha = 1.1$ and uniform injection rate of water vapor, and $\alpha = 1.1$ but injection favoring the high troposphere, respectively. The fourth and fifth rows exhibit the model runs with vertical transport by eddy diffusion, D with $\alpha = 1.1$ and $D_{\alpha(T)}$ with $\alpha(T)$. For further comparison the right panel in the third row shows a mixing curve between the highest and lowest data point.

[50] This raises, however, two interesting questions. The first is, Why is the assumption of a constant α of 1.1 so successful in simulating the observed D content up to altitudes of 9 km? This question will be addressed in section 4.6.

[51] The second is, Why does a model, which provides vertical mixing, generate a dependence so close to that of a Rayleigh condensation curve? The answer for the second question is twofold: The first is of course that the D content of the primary injection which replenishes the tropospheric water vapor is governed by Rayleigh condensation. The second is that the rate of injection is uniform with altitude and that each injection event is followed by a corresponding downward motion throughout the air column below. Accordingly, the mixing generated by the downward motion in model C1 is unidirectional and stepwise, incorporating air with a lower D and lower water content from each level above to the next lower one. It thus acts along a mixing curve between two adjacent altitude levels, which keeps the δ_v/q_v relation close to and slightly above that for Rayleigh condensation (an example of a mixing curve is given in the right panel for run C2 in Figure 9).

[52] The effect of the downward mixing of dryer air is, however, clearly visible in the profile of relative humidity for C1, which averages about 43% over the altitude range considered, whereas injection alone would maintain the air at h = 100%.

[53] The other simulation runs of δ_v illustrate the sensitivity of the results to the assumptions made on injection profile, fractionation factor, and mode of transport. Model run C2 demonstrates the impact of a drastically different injection profile: injecting surface air preferentially into the uppermost troposphere. Both the δ_v/q_v dependence and the h profile generated by C2 differ significantly from the observations and C1. The effect on the δ_v/q_v dependence, however, turns out to be relatively minor with a slightly stronger bulge to higher D contents maximizing at a water vapor mixing ratio of about 1 g/kg, i.e., in the direction of a hypothetical mixing curve which mixes air from the surface, $\delta_D = -135‰$, $q_{v,0} = 8$ g/kg and air from 9 km altitude, $\delta_D = -345‰$, $q_v = 0.38$ g/kg (see C2 panel in Figure 9). The impact of the different injection profile on the h profile is much stronger: The preferential injection by C2 at the low temperatures in the upper troposphere introduces more air with low water vapor mixing ratios, and the subsequent downward transport of this air dries the levels below more effectively.

[54] Run D demonstrates that transport by eddy diffusion provides a mixing that decreases the gradient in the δ_v/q_v dependence considerably. The modeled curve retains the functional form of a Rayleigh condensation but with a fractionation factor of $\alpha^{0.5}$ only. This was already pointed out by *Eriksson* [1965]. Clearly, run D with $\alpha = 1.1$ differs greatly from C1 and does not explain the observations.

[55] These comparisons highlight the major factors that control the average local vertical profile of the D content: These are the lower boundary conditions of the D content and humidity (the upper boundary, if placed within the stratosphere, plays virtually no role); the vertical profile of α; the type of vertical transport and the degree of mixing provided by it; and the vertical injection pattern. Of course any observed individual profile, as well as the average ones, may also be influenced by horizontal advection, which is not captured by a 1-D model.

[56] Finally we note that case C1, i.e., vertical transport by lofting and a constant α, would, among the cases considered, also best explain the uncorrected summer data over Scotts Bluff (see Figure 4c), albeit with a slightly smaller α. If one allowed for a variable α, it would have to decrease with altitude to explain the uncorrected D content of the highest samples. By the same token, if the present correction method led to an over correction, the constant α derived from modeling case C1 would represent a slight overestimate.

4.6. Effective Fractionation

[57] Already *Merlivat and Jouzel* [1979] demonstrated that inside a precipitating cloud, in a situation where condensate is lofted along with water vapor, the effective fractionation is less than that expected from the equilibrium $\alpha(T)$. The reason for this is easily recognized by the following consideration.

[58] When air containing also condensate is lofted, the amount of water carried upward and remaining in the atmosphere is given by

$$q_t = q_v + q_c \tag{8}$$

and its D content is given by

$$q_t \times R_t = q_v \times R_v + q_c \times R_c \tag{9}$$

where $R = HDO/H_2O$; q refers to the amounts of water in the different phases. The subscripts t, c, v stand for total, condensate, and vapor, respectively.

[59] As part of the condensate is removed with an isotope content which is by definition R_c, the remaining total water experiences a fractionation given by an effective fractionation factor

$$\alpha^* = R_c/R_t \tag{10}$$

rather than by the equilibrium factor

$$\alpha(T) = R_c/R_v = p_{H_2O}/p_{HDO}, \tag{1'}$$

as it would if no condensate was lofted.

[60] Inserting equations (8) and (9) into equation (10) and adopting (1′) for the fractionation between vapor and condensate, one obtains

$$\alpha^* = \frac{\alpha(T)}{1 + [\alpha(T) - 1] \cdot q_c/q_t} \tag{11}$$

Clearly for $q_c \to 0$, $\alpha^* \to \alpha(T)$, and for $q_c \to q_t$, $\alpha^* \to 1$.

[61] For any finite amount of q_c, which in a precipitating cloud may range from 0.1 g/kg to 1 g/kg, $\alpha^* < \alpha(T)$. In our model runs, where $q_{v,o} = 8$ g/kg and $q_v(9\text{ km}) = 0.4$ g/kg, the assumption of a $q_c = 0.5$ g/kg constant with altitude leads to a profile of α^* of 1.09 at the lowest condensation altitude, 1.08 at the highest altitude (9 km), and a maximum of 1.11 at about 5 km with an mean value of 1.1 when averaged over the whole profile, whereas $\alpha(T)$ exhibits a monotonic

increase from 1.09 to 1.21 over the same height interval. Thus an $\alpha^* = 1.1$ approximately constant over the altitude range from 1.2 to 9 km altitude as sampled in summer over Scotts Bluff is not implausible.

[62] This derivation of α^* assumed thermodynamic equilibrium between the condensed and vapor phase. Thus the simple form of equation (11) will not be applicable when the condensed phase consists of ice and equilibrium cannot be reached, because the inner layers are shielded from contact with vapor by those deposited later. Still the general conclusion of the effective fractionation factor approaching the value of 1 for $q_c \gg q_v$ remains valid in this case too. As the amount of ice dominates over that of water vapor, its isotope content will also dominate that of the remaining moisture, and α^* as defined by equation (10) will approach unity. From thereon fractionation ceases. Hence in the highest layers of the troposphere, where water vapor is replenished by evaporation of lofted ice crystals [*Keith*, 2000; *Dessler and Sherwood*, 2003], the vertical gradient in the D content could vanish.

[63] The α^* so far considered depends only on the microphysics in a cloud. It would be applicable in any type of model or any actual situation. In many instances it alone is sufficient to explain why the apparent α in an observed δ_v/q_v relation has a value as low as 1.1.

[64] However, in the case of the seasonally averaged δ_v/q_v dependence or in the 1-D models, the one parameter α must encapsulate all processes that contribute to fractionation. This leads to further modifications in α. We have already seen that the mixing provided by eddy diffusion in run D reduces the fractionation apparent in the δ_v/q_v dependence from the α inherent in the removal to an apparent fractionation factor of $\alpha^{0.5}$. Thus turbulent mixing provides another reduction in the apparent α as utilized in the convection model. In a real situation with mean currents along with turbulent mixing, the exponent in α would range between 0.5 and 1, and thus the reduction in the apparent α is smaller than in run D. There are, however, still other processes influencing the overall fractionation, such as the isotopic mixing provided by precipitation falling back into the lofted air. As a consequence the apparent α derived from the seasonally averaged δ_v/q_v dependences and the α in the 1-D models are rather convoluted parameters with contributions from several processes. Nevertheless, as we have shown, a simple convection model with a single parameter α is quite capable of simulating average vertical profiles of the D content as well as its dependence on the water vapor mixing ratio up to an altitude of 9 km at midlatitudes.

5. Summary and Conclusions

[65] We reanalyzed the measurements of the D content in tropospheric water vapor presented by *Ehhalt* [1974]. Although these measurements date far in the past and lack the auxiliary measurements to determine the amount and D content of contaminating wall water in the sampling tubes, we were able to devise a satisfactory correction procedure for that contamination. Original and corrected data are available at http://www.atd.ucar.edu/apol/ehhalt/Vertical_Profiles_of_HDO.html. The resulting corrections decreased the D content. They were relatively small for the data from the flights prior to 1968, which reached from the surface to 9 km altitude.

[66] The corrected D data were presented in the form of seasonally averaged vertical profiles and, again seasonally averaged, as function of the measured water vapor mixing ratio for the locations Scotts Bluff, Death Valley, and Pacific. The vertical profiles showed the expected decrease of the D content with altitude and seasonal variation at all altitudes albeit with substantial scatter for the two latter locations. Interestingly, when plotted as a function of the log of the water vapor mixing ratio, a large part of the data from all seasons and locations collapsed on a line which closely followed that given by a Rayleigh condensation curve with a fractionation factor $\alpha = 1.1$, constant with altitude, a conclusion which by the way does not depend on the corrections.

[67] A simple one-dimensional convection model, which lofts air from the surface layer directly into the layers between 1 and 12 km altitude and subjects the lofted water vapor to isotope fractionation by Rayleigh condensation with $\alpha = 1.1$, explained the summer observations surprisingly well. The choice of a constant (and not thermodynamic) fractionation factor was explained largely by cloud and precipitation elements in the amount of 0.5 g/kg lofted along with the water vapor.

[68] At higher altitudes the lofting of ice particles decreases the effective fractionation factor asymptotically to 1. As a result the vertical decrease of water vapor at those altitudes becomes vanishingly small [see also *Keith*, 2000].

References

Craig, H. (1961), Standard for reporting concentrations of deuterium and oxygen-18 in natural waters, *Science*, *133*, 1833–1834.

Dessler, A. E., and S. C. Sherwood (2003), A model of HDO in the tropical tropopause layer, *Atmos. Chem. Phys.*, *3*, 2173–2181.

Dushman, S. (1962), *Scientific Foundations of Vacuum Technique*, John Wiley, Hoboken, N. J.

Ehhalt, D. H. (1974), Vertical profiles of HTO, HDO, and H_2O in the troposphere, *NCAR Tech. Note NCAR–TN/STR–100*, 131 pp., Natl. Cent. for Atmos. Res., Boulder, Colo.

Ehhalt, D. H., and H. G. Östlund (1970), Deuterium in Hurricane Faith 1966: Preliminary results, *J. Geophys. Res.*, *75*, 2323–2327.

Ehhalt, D. H., F. Rohrer, and A. Wahner (1992), Sources and distribution of NO_x in the upper troposphere at northern mid-latitudes, *J. Geophys. Res.*, *97*, 3725–3738.

Ehhalt, D. H., F. Rohrer, S. Schauffler, and W. Pollock (2002), Tritiated water vapor in the stratosphere: Vertical profiles and residence time, *J. Geophys. Res.*, *107*(D24), 4757, doi:10.1029/2001JD001343.

Eriksson, E. (1965), Deuterium and oxygen-18 in precipitation and other natural waters: Some theoretical considerations, *Tellus*, *27*, 498–512.

Friedman, I. (1953), Deuterium content of natural waters and other substances, *Geochim. Cosmochim. Acta*, *4*, 89–103.

Gedzelman, S. D. (1988), Deuterium in water vapor above the atmospheric boundary layer, *Tellus, Ser. B*, *40*, 134–147.

Keith, D. W. (2000), Stratosphere–troposphere exchange: Inferences from the isotopic composition of water vapor, *J. Geophys. Res.*, *105*, 15,167–15,173.

Kley, D., J. M. Russell III, and C. Phillips (Eds.) (2000), Assessment of upper tropospheric and stratospheric water vapour, *WCRP 113, WMO/TD–1043, Rep. 2*, Stratospheric Processes and their Role in Clim. (SPARC), Toronto, Ont., Canada.

Knight, C. A., D. H. Ehhalt, N. Roper, and N. Knight (1975), Radial and tangential variation of deuterium in hailstones, *J. Atmos. Sci.*, *32*, 1990–2000.

Kuang, Z., G. C. Toon, P. O. Wennberg, and Y. L. Yung (2003), Measured HDO/H_2O ratios across the tropical tropopause, *Geophys. Res. Lett.*, *30*(7), 1372, doi:10.1029/2003GL017023.

Lawrence, J. R., S. D. Gedzelman, J. Gamache, and M. Black (2002), Stable isotope ratios: Hurricane Olivia, *J. Atmos. Chem.*, *41*, 67–82.

Majoube, M. (1971), Fractionnement en oxygène 18 et en deuterium entre l'eau et sa vapeur, *J. Chim. Phys. Phys. Chim. Biol.*, *10*, 1423–1436.

Merlivat, L., and J. Jouzel (1979), Global climatic interpretation of the deuterium–oxygen 18 relationship for precipitation, *J. Geophys. Res.*, *84*, 5029–5033.

Merlivat, L., and G. Nief (1967), Isotopic fractionation of the solid-vapor and liquid-vapor changes of state of water at temperatures below 0°C, *Tellus*, *19*, 122–127.

Rozanski, K., and C. Sonntag (1982), Vertical distribution of deuterium in atmospheric water vapor, *Tellus*, *34*, 135–141.

Smith, R. B. (1992), Deuterium in North Atlantic storm tops, *J. Atmos. Sci.*, *49*, 2041–2057.

Webster, C. R., and A. J. Heymsfield (2003), Water isotope ratios D/H, $^{18}O/^{16}O$, $^{17}O/^{16}O$ in and out of clouds map dehydration pathways, *Science*, *302*, 1742–1745.

Zahn, A. (1995), Der Tracertransport in der Tropopausenregion, Ph.D. thesis, 215 pp, Inst. für Umweltphysik, Univ. Heidelberg, Heidelberg, Germany.

Zahn, A., V. Barth, K. Pfeilsticker, and U. Platt (1998), Deuterium, oxygen-18, and tritium as tracers for water vapour transport in the lower stratosphere and tropopause region, *J. Atmos. Chem.*, *30*, 25–47.

D. H. Ehhalt and F. Rohrer, Forschungszentrum Jülich, ICG-II: Troposphäre, 52425 Jülich, Germany. (f.rohrer@fz-juelich.de)

A. Fried, Atmospheric Technology Division, National Center for Atmospheric Research, 3450 Mitchell Lane, Boulder, CO 80301, USA.